Single-cell mapping links neurogenesis and angiogenesis in aggressive breast cancer

Elisabeth Wik[1,2#], Sura Aziz[1,2#], Kenneth Finne[1], Dimitrios Kleftogiannis[1,5], Cecilie Askeland[1,2], Gøril Knutsvik[1,2], Kristi Krüger[1], Amalie A. Svanøe[1], Even Birkeland[1,3], Silje Kjølle[1], Benedicte Davidsen[4], Ingunn M. Stefansson[1,2], Heidrun Vethe[1], Lars A. Akslen[*1,2]

[#] *These authors contributed equally*

[1] Centre for Cancer Biomarkers CCBIO, Department of Clinical Medicine, University of Bergen, Bergen, Norway.
[2] Department of Pathology, Haukeland University Hospital, Bergen, Norway.
[3] Department of Biomedicine, University of Bergen, Bergen, Norway
[4] Department of Surgery, Haukeland University Hospital, Bergen, Bergen, Norway.
[5] Computational Biology Unit (CBU), Department of Informatics, University of Bergen, Bergen, Norway

---

*** Corresponding author:**

Prof. Lars A. Akslen, MD PHD
Centre for Cancer Biomarkers CCBIO
Department of Clinical Medicine
Section for Pathology, University of Bergen,
Bergen, Norway
Email: lars.akslen@uib.no
Tel: +4755973182

Conflict of interest statement:

The authors have declared that no conflict of interest exists.

Abstract

The tumor microenvironment (TME) is important for cancer growth and progression. While angiogenesis is an established hallmark of cancer, the role of nerve fibers is less studied. Here, we investigated neurogenesis and angiogenesis in breast cancer and found them to be closely associated. Single-cell based spatial mapping by imaging mass cytometry (IMC) indicated close proximity between neural and vascular structures. Subsequent validation by tissue-based markers of neurogenesis and angiogenesis, supported by proteomics and transcriptomics data of tissues and cell lines, supported a link between these processes. A consolidated neuro-angiogenic signature score was linked to high-grade breast cancer and reduced patient survival, also within the low-grade luminal tumor subgroup. Our findings support that neurogenesis and angiogenesis are related in aggressive breast cancer and might possibly improve tumor stratification and clinical management.

Introduction

Tumor-stroma communication is important for cancer progression and is suggested as a therapeutic target. Programs of inflammation, angiogenesis, and fibroblast activation are among the tumor microenvironment (TME) characteristics of aggressive cancer (1, 2). Recently, evidence has indicated links between tumor cells, nerve elements and progressive disease (3, 4), and experimental studies suggest that cancer cells may simultaneously promote the recruitment of both sprouting axons and endothelial cells(5-9). However, studies of neural tissue in breast cancer stroma are limited (10-16), and the potential coexistence of microaxons and microvessels have, to our knowledge, not been examined in human tumor tissues.

Here, single-cell imaging mass cytometry (IMC), combined with mass spectrometry-based proteomics and transcriptomics data from different human breast cancer cohorts, were investigated for the relationship between neural and vascular processes in breast cancer TME. Our findings support the notion that neurogenesis and angiogenesis are linked in aggressive breast cancer and associated with clinical outcome. These results provide a basis for improved tumor stratification and more precise clinical management of breast cancer patients.

Methods

Patient series

The study cohort included women diagnosed with primary invasive breast cancer as part of the prospective and population-based Norwegian Breast Cancer Screening Program during 1996-2003 (Hordaland County, Norway; 10% of the Norwegian population), age 50–69 years at time of diagnosis (median 59 years). Detailed information about this study population and the specimen characteristics is presented in Supplementary Material.

Imaging mass cytometry (IMC)

IMC breast cancer cohort. We analyzed tissues from two independent tissue collection studies (n=117). Cohort-1 consisted of tumors from the Norwegian Breast Cancer Screening Program. Cohort-2 was established in collaboration with Prof.

William D. Foulkes at McGill University, Canada. We assessed both cohorts using tissue microarrays (TMAs) with 1mm cores in triplets and analyzed one core from each patient.

IMC antibody panel. The antibody panel consisted of 36 metal-conjugated antibodies. All antibodies were validated by IHC using a test-TMA with positive control tissues. A pilot-TMA was established to validate and calibrate the experimental protocol. Antibody hybridization was performed as described by Fluidigm with a few modifications (see Supplementary Material).

IMC acquisition and data pre-processing. Data from the IMC cohort (n=117) were acquired by a Helios time-of-flight mass cytometer (CyTOF) coupled to a Hyperion Imaging System (Fluidigm) and administered using the CyTOF Software (v7.0.8493; Fluidigm). The square inscribed in the circular TMA cores were laser ablated at 200 Hz at a resolution of approximately 1µm^2. Detailed information of the cell segmentation and IMC analysis workflow can be found in Supplementary Material.

Nerve and vessel density measurements by IHC

Sections from primary tumors and the matched axillary node with the largest metastatic focus (≥ 2 mm) were used for assessment of nerves (Neurofilament antibody, DAKO M0762), and angiogenesis markers (Factor-VIII, DAKO A0082; Ki67, DAKO 7240). Vessels from adjacent normal tissue were used as controls. For further details on immunohistochemistry and assessment of nerve- and vessel density measurements (MAD, NBD, MVD and pMVD), see Supplementary Material.

Proteomic and mRNA datasets

In this study we have used in-house datasets: Microdissected breast cancer epithelial tissue (proteomics, n=24), Secretome from breast cancer cell lines (proteomics, n=4), Cell line lysate (mRNA, n=12), and external datasets: METABRIC (mRNA, discovery cohort, n=939; validation cohort, n=845; normal-like excluded), CCLE (mRNA, n=47) and a recently published proteomics dataset by Asleh and colleagues (17) (proteomics, n=284). For more information see Supplementary Material.

Statistics and survival analyses

Data were analyzed using SPSS (Statistical Package for the Social Sciences), Version 28.0 (Armonk, NY, USA; IBM Corp) and R-packages via Rstudio v1.3.9. A

two-sided P-value less than 0.05 was considered statistically significant. Detailed descriptions of the statistical methods can be found in Supplemental Material)

Study approval

This study was approved by the Western Regional Committee for Medical and Health Research Ethics, REC West (REK 2014/1984). Written informed consent was not obtained from the patients, but in accordance with national ethics guidelines and procedures for retrospective studies, all participants were contacted with written information on the study and asked to respond if they objected. In total, 9 patients (1.7%) did not approve of participation.

Results

Single-cell mapping of breast cancer tissue by imaging mass cytometry indicates neuro-vascular proximity

To investigate the single-cell spatial distribution and potential co-localization of neural and vascular structures in breast cancer, we designed an IMC panel of 36 markers (**Supplementary Table 1**) to profile 117 samples from luminal A (n=26), luminal B (n=30), HER2 enriched (n=9) and triple-negative tumors with a basal-like phenotype (n=52). In total, we identified 413,271 single cells or equally denoted cell units (*i.e.*, 218,117 from basal-like and 195,154 from luminal-like tissues), quantifying marker expression combined with spatial information of each cell unit. Initially, unsupervised clustering was used to identify basic cell phenotypic clusters of different epithelial phenotypes, T-cells, B-cells, macrophages, endothelial cells, and stromal cells (18).

We used IMC-based images to detect areas with spatial co-localization of neural and vascular structures (**Figure 1a-b**). For each endothelial cell unit, we estimated the number of neighboring cells using a k-nearest approach, and we visualized the average distance from all cell units with high Neurofilament (NF) marker expression.

To elucidate whether markers of neural units and vasculature are closely localized, we used density estimation of the Neurofilament (NF) marker from low to high expression (**Figure 1c**). Vascular proliferation was determined by CD31CD34 expressing endothelial cells based on high or low Ki67 expression using density estimates from the flowDensity software (19), resulting in two subsets: Ki67-

high/CD31CD34+ and Ki67-low/CD31CD34+. We observed that proliferating vessels (Ki67-high/CD31CD34) were clearly distinct in the 2D space from non-proliferating endothelial cells (Ki-67-low/CD31CD34+) (**Figure 1d**).

Comparing the overall distribution of NF expressing cell units associated with endothelial cell subsets (Ki67-high/CD31CD34+ and Ki67-low/CD31CD34+) indicated that NF expression was on average higher in association with proliferative endothelial cell units (Ki67-high/CD31CD34+) than in Ki67-low/CD31CD34+ ($P<0.001$) (**Figure 1e**). Distance analysis indicated that NF-high cells were significantly closer to proliferative endothelium (**Figure 1f)** ($P<0.001$) suggesting an association of neurogenic and angiogenic structures and the potential presence of tumor associated neuro-vascular niches.

Taken together, our spatial single-cell analysis revealed that markers reflecting neurogenesis (NF+) and angiogenesis (Ki67-high/CD31CD34+) are co-localized, supporting a relationship which might hold functional importance. To assess the potential clinical relevance of our findings, we further mapped neural and vascular structures and signatures at the case-level in breast cancer using immuno-histochemistry (IHC) and omics data.

Neural and vascular tissue markers in primary and metastatic breast cancer associate with aggressive tumor features

For case-based validation of neural and vascular structures in breast cancer, we applied IHC staining for NF and Factor-VIII on tissues from 534 primary cases and 95 matched lymph node metastases.

Among 483 primary tumors with sufficient tissue for examination (90%), microaxons were detected in 102 (21%) cases (**Figure 2a**) and nerve bundles in 126 (26%) cases (**Figure 2b**). We found a median MAD (microaxon density) of 0.058 per mm^2 and median NBD (nerve bundle density) of 0.080 per mm^2. Presence of microaxons associated with features of aggressive BC (**Table 1**), whereas no associations were observed between expected pre-existing nerve bundles and primary tumor features. Further, in lymph node (LN) metastases (n=58, after exclusion of micrometastases and cases with insufficient material), microaxons were present in 36 (62%) of metastatic lymph nodes with MAD exhibiting reduced values compared to matched primary tumors ($P=0.001$). Microaxons in LN metastases associated with features of

aggressive BC; (**Supplementary Table 2**); nerve bundles were not detected in lymph nodes with metastases.

We then examined markers of vascular structures (**Figure 2c-d**), *i.e.,* microvessel density (MVD), vascular proliferation (pMVD) and VPI (vascular proliferation index; pMVD/MVD x 100). Among 461 primary tumors, we found a median pMVD of 3.07 per mm^2, median VPI of 3.5 %, and median MVD of 77.6 per mm^2. High pMVD and VPI scores showed associations with features of aggressive tumors, and scores were higher in HER2 positive, triple negative and basal-like subtypes (**Table 2**). Results for LN metastases paralleled the primary tumors (**Supplementary Table 3**). Scores of pMVD and VPI reflecting active angiogenesis had higher values in primary tumors as compared to matched LN metastases (**Supplementary Table 4**). Within each molecular subtype, we also found that the VPI scores were higher in primary tumors as compared to matched LN metastases (**Supplementary Table 5**).

Further, we observed that presence of microaxons was positively correlated with pMVD and VPI, while no correlation was detected with MVD scores (**Supplementary Figure 1a-c**). Higher VPI scores were observed in primary tumors with microaxons ($P<0.001$), when combining all molecular subtypes together as well as for Luminal A and Luminal B/HER2 (**Figure 2e**).

To investigate whether presence of neural and vascular markers associate with patient survival, we performed univariate analysis using the Kaplan-Meier method. Higher vascular proliferation measured by VPI score in primary tumors were associated with shorter survival (**Figure 2f)**, whereas there was no difference in patient survival for MVD score. Increased vascular proliferation measured by VPI in LN metastases indicated reduced survival ($p=0.05$; **Figure 2g**). Notably, low VPI in primary tumors indicated improved survival within the basal-like category ($p=0.05$).

When including VPI in multivariate survival analysis using Cox modelling, adjusting for traditional prognostic factors (tumor diameter, histologic grade, lymph node status), VPI maintained independent prognostic value (**Supplementary Table 6**).

MAD measured in the primary tumors did not stratify patients in groups of significantly different survival (**Figure 2h**). However, in LN metastases, we observed that presence of MAD associated with reduced survival (**Figure 2i**).

Proteomic analysis indicates differential expression of neural and vascular proteins in breast cancer tissues and cells

Using our subcohort of microdissected cases (in-house tissues, tumor epithelial component: 12 basal-like, 12 luminal-like breast cancers), our data indicated 967 differentially enriched proteins when comparing basal-like and luminal-like cases (**Supplementary Table 7; Figure 3a**), of which 26 proteins were involved in *axonogenesis* (n=473; gene-sets GO:0007409); we termed these 'neurogenesis-related' proteins. Moreover, 17 angiogenesis-related proteins (n=494; gene-set GO:0001525) were also differentially expressed between basal-like and luminal-like breast cancer cases. The neurogenesis and angiogenesis related proteins were combined into a 'neurogenesis-angiogenesis signature' of 43 proteins (NAS-43).

To probe whether our protein expression profiles could be characteristic for aggressive tumor features, we quantified the NAS-43 proteins using independent datasets from three different sources, in addition to our in-house dataset of microdissected breast cancer cells from which NAS-43 was derived (n=24; **Figure 3b**); 1) a previously reported proteomics profiling of 284 breast cancer cases (17) (**Figure 3c**); 2) a proteomic dataset of 30 BC cell lines from the CCLE (20) (**Figure 3d**), and 3) an in-house secretome dataset derived from four cell lines (**Figure 3e**). Using simple unsupervised hierarchical case clustering, we observed clear separation of basal-like and luminal-like cases (based on Dunn and Silhouette indexes for clustering quality evaluation), see **Supplementary Figure 2)**. Taken together, our data indicate that expression profiles of proteins related to neurogenesis and angiogenesis separate basal-like from luminal-like breast cancer subtypes for patient data (microdissected or whole tissues) and cell line information (whole cells or secretomes).

We found the expression of neurogenic and angiogenic proteins, derived from our microdissected breast cancer cohort, to be significantly associated (**Supplementary Figure 3a**). Further, the merged neuro-angiogenic proteomic signature (NAS-43) associated significantly with our NAS signature, a combined neuro-angiogenic mRNA based signature (described below), thus validating a tight association between neurogenic and angiogenic expression profiles (METABRIC cohort; **Supplementary Figure 2b**). Notably, the NAS-43 signature was significantly associated with patient

survival as shown in both METABRIC and KMplotter cohorts, in all patients and within the luminal A subgroups (**Figure 4**).

When broadening the focus by assessing neurogenesis and angiogenesis-relevant proteins (n=43) in the independent patient cohort of Asleh et al. (n=284) (17), we found heterogeneity of whole-tissue breast cancer samples. Using simple hierarchical clustering, most of the luminal A cases resided in the same tree branch which was clearly distinct from the basal-like cases. As expected, some luminal B cases and HER2-enriched tumors were clustered together with the main molecular subtypes reflecting the underlying biological characteristics. Our proteomics profiling of neurogenesis and angiogenesis related proteins are in concordance with our IMC and IHC data, providing additional evidence of neurogenic and angiogenic differences between basal-like and luminal-like subtypes.

Gene expression analysis support neurogenesis and angiogenesis as features of aggressive breast cancer

To further elucidate how gene expression patterns representing neurogenesis and angiogenesis relate to breast cancer phenotypes and tumor progression, we used two previously reported mRNA expression signatures reflecting stroke-related sprouting axons(21) for neurogenesis, and vascular proliferation previously associated with increased microvessel proliferation in endometrial cancer(22) for angiogenesis, examined in the METABRIC cohort (n=1710) combined with breast cancer cell line data from CCLE (n=59) and in-house cell line secretome experiments (12 cell lines; 6 luminal, 6 basal).

On average, sprouting axon score (SAS) and vascular proliferation score (VPS) were higher in basal-like breast cancer as compared to luminal A, luminal B and Her2 enriched subtypes ($P<0.001$) (**Supplementary Figure 4a-b).** To investigate the combined effect of SAS and VPS, and since these signatures were significantly associated, we merged the scores creating a new Neuro-Angio score (NAS) (see Methods). As expected, NAS showed distinct separation between molecular BC subtypes (**Supplementary Figure 4c).** Considering both METABRIC and CCLE data, we found significant and strong positive correlations between SAS and VPS at the gene expression level (**Supplementary Figure 4d-e)**. The highest NAS was seen in basal-like breast cancer (**Supplementary Figure 4c-f**)**.** Adding more information at

the global transcriptomic level, these observations are in concordance with our findings from IMC and IHC, and our data support an association between neurogenesis and angiogenesis in aggressive breast cancer subtypes.

We then investigated patient survival using this additional layer of information in the METABRIC data. Patients with high SAS and high VPS were associated with reduced survival (**Supplementary Figure 4g-h**). For the combined NAS, we found associations with shorter survival, both in univariate (**Supplementary Figure 4i**) and multivariate analysis, adjusting for basic factors tumor diameter, histologic grade, and lymph node status (**Supplementary Figure 4j**). When adding PAM50-based molecular subtype to the multivariate model, high NAS independently predicted reduced survival (METABRIC: HR=1.4; 95% CI 1.1-1.7; P=0.001). High NAS maintained independent association with survival within luminal tumors (HR=1.39; 95% CI 1.05-1.84; P=0.022), with a similar trend in non-luminal tumors (P=0.09), when adjusting for tumor diameter, histologic grade, and lymph node status.

Further supporting our finding that NAS was related to aggressive tumor features, associations were found between NAS-score and mRNA-based signatures for EMT, TGFb, stem cell features, and hypoxia, in both METABRIC and TCGA cohorts (**Supplementary Figures 5-6**). When clustering dichotomized signature scores reflecting EMT, stemness, and hypoxia, along with phenotypic clinico-pathologic markers in accordance with high or low NAS, phenotypic subgroups among tumors were evident (four clusters, C1-C4; **Figure 5a-b)**. Two of these clusters (C2, C4) had significant prognostic impact independent of the PAM50 classifier and other basic factors (METABRIC cohort) (**Figure 5c**).

Discussion

The influence of the microenvironment on tumor progress has been increasingly recognized (23-25). Since the link between neurogenesis and angiogenesis has not been well addressed in human cancer, we asked whether these processes are associated traits and related to more aggressive features of breast cancer. By using single-cell tissue analytics in combination with proteomics and transcriptomics data from patients and cell lines, our findings indicate a connection between neural and

vascular structures in these tumors, supporting a neuro-vascular niche concept with potential functional implications. Single-cell mapping of breast cancer tissues demonstrated associations between NF expressing cell units and proliferating vessels, and NF+ cells were significantly closer to these proliferating vascular structures compared with the Ki67-low/CD31-CD34+ vessels.

Spatial single-cell mapping of neural and vascular structures indicated significant proximity. Experimental studies have indicated commonalities for neuronal guidance and vascular sprouting, supporting that the two processes might be co-regulated (7, 8), although this has not been previously addressed in human cancer tissues. Future studies will explore a possible functional relationship between neural and vascular components in human breast cancer.

Tumor-associated neurogenesis was strongly associated with markers of high-grade tumors, such as negative hormone receptors, evidence of tumor cell plasticity, and stemness features. The highest level of microaxon density was found in basal-like and Her2 positive breast cancers, while the lowest density was observed in the luminal A subgroup, supporting recent data (15). Nerve bundles, assumed to be pre-existing structures, were observed in many primary tumors but did not associate with any high-grade tumor traits. Such nerve bundles were not observed in lymph node metastases, where microaxons might possibly develop *de novo* from circulating or tissue resident cells (26). Patient survival was reduced in cases with presence of microaxons in lymph node metastases.

At the proteomic and transcriptomic level, combined neuro-angiogenic scores (NAS and NAS-43) was linked to high-grade breast cancer and independently related to reduced patient survival by multivariate analysis. The neuro-angiogenic signature was even stronger than the tumor cell-based classification.

When exploring multiple breast cancer cell lines (27), higher levels of the neuro-angiogenic score were observed in the most aggressive cancer subtypes. This indicates that neuro-angiogenic programs appear to be part of intrinsic tumor cell properties. Taken together, the fact that the neuro-angiogenic score was prognostic within the luminal-like breast cancers, and the finding that some of the cases with high neuro-angiogenic score were hormone receptor positive, might indicate discordant evolution of tumor cells and TME in subsets of breast cancer.

Tumor angiogenesis is an established *hallmark of cancer* (1) and is well described in breast tumors (28, 29). Here, we found consistent and strong associations between proliferating vasculature and aggressive breast cancer phenotypes. Vascular proliferation was increased in basal-like cancers, as we have reported previously(29, 30). As a novel finding, low vascular proliferation within the subgroup of aggressive basal-like cancers indicated a better prognosis compared to the others. Also, elevated vascular proliferation examined in lymph node metastases was associated with reduced survival, which has not been previously reported.

In summary, our data support that neurogenesis and angiogenesis are associated features of aggressive breast cancer. High neuro-angiogenic score was consistently linked to high-grade breast cancer phenotypes and reduced patient survival. Notably, among some hormone receptor positive cases, a high-grade subgroup could be defined by increased neuro-angiogenic score. Single-cell tissue mapping indicated close proximity of neural and proliferating vascular structures, suggesting the possibility of neuro-vascular niches in the tumor microenvironment. Taken together, our findings might be relevant for improved patient stratification and exploration of novel therapy.

Author contribution

LAA conceived and designed the study and contributed to histologic analyses (IHC, IMC), data interpretation and in writing the major parts of the manuscript. EW contributed to the study design, analyzing the transcriptomic data, general data analyses and interpretation, and in writing the major parts of the manuscript. SA contributed to the study design, performed the tissue-based work and IHC, performed statistical analysis, data interpretation and contributed to writing the manuscript. DK contributed to study design and analyzing the mRNA and IMC data, and contributed to writing the manuscript. HV and KF contributed to analyses of proteomics and IMC data. CA contributed to histologic analyses and work on IMC data, and to collection of clinico-pathologic data. GK participated in data collection and interpretation. KK, AAS, EB, SK, and IMS participated in data collection and interpretation. BD participated in collection of clinical data. All authors commented on and approved the final manuscript. EW and SA made the initial core findings, whereas EW played a

larger role in manuscript completion; thus, EW is listed first in the authorship. All authors have read and approved the submitted paper.

Acknowledgements and funding information

We thank Gerd Lillian Hallseth and Bendik Nordanger for their excellent technical assistance. This work was partly supported by the Research Council of Norway through its Centre of Excellence funding scheme, project number 223250. The study was also supported by the Norwegian Cancer Society and Regional Health Trust Western Norway (Helse Vest).

Data availability statement

In-house proteomics and transcriptomics data will be made available through online repositories (PRIDE and Gene Expression Omnibus, respectively), and R scripts will be available through GitHub, at the time of publication. Clinical data from patients included in this study may be made available to researchers upon request after completion of a Data Transfer Agreement and confirmation of ethical approval.

Conflicts of interest

The authors declare no competing interests.

References

1. Hanahan D, Weinberg RA. Hallmarks of cancer: the next generation. Cell 2011;144(5):646-74.
2. Hanahan D. Hallmarks of Cancer: New Dimensions. Cancer Discov 2022;12(1):31-46.
3. Hayakawa Y, Sakitani K, Konishi M*, et al.* Nerve Growth Factor Promotes Gastric Tumorigenesis through Aberrant Cholinergic Signaling. Cancer Cell 2017;31(1):21-34.
4. Monje M, Borniger JC, D'Silva NJ*, et al.* Roadmap for the Emerging Field of Cancer Neuroscience. Cell 2020;181(2):219-222.
5. Mancino M, Ametller E, Gascon P, Almendro V. The neuronal influence on tumor progression. Biochim Biophys Acta 2011;1816(2):105-18.
6. Entschladen F, Palm D, Lang K*, et al.* Neoneurogenesis: tumors may initiate their own innervation by the release of neurotrophic factors in analogy to lymphangiogenesis and neoangiogenesis. Med Hypotheses 2006;67(1):33-5.
7. Magnon C, Hall SJ, Lin J*, et al.* Autonomic nerve development contributes to prostate cancer progression. Science 2013;341(6142):1236361.
8. Zahalka AH, Arnal-Estape A, Maryanovich M*, et al.* Adrenergic nerves activate an angio-metabolic switch in prostate cancer. Science 2017;358(6361):321-326.
9. March B, Faulkner S, Jobling P*, et al.* Tumour innervation and neurosignalling in prostate cancer. Nat Rev Urol 2020;17(2):119-130.

10. Zhao Q, Yang Y, Liang X, *et al.* The clinicopathological significance of neurogenesis in breast cancer. BMC Cancer 2014;14:484.
11. Lagadec C, Meignan S, Adriaenssens E, *et al.* TrkA overexpression enhances growth and metastasis of breast cancer cells. Oncogene 2009;28(18):1960-70.
12. Reis-Filho JS, Steele D, Di Palma S, *et al.* Distribution and significance of nerve growth factor receptor (NGFR/p75NTR) in normal, benign and malignant breast tissue. Mod Pathol 2006;19(2):307-19.
13. Tomellini E, Touil Y, Lagadec C, *et al.* Nerve growth factor and proNGF simultaneously promote symmetric self-renewal, quiescence, and epithelial to mesenchymal transition to enlarge the breast cancer stem cell compartment. Stem Cells 2015;33(2):342-53.
14. Huang D, Su S, Cui X, *et al.* Nerve fibers in breast cancer tissues indicate aggressive tumor progression. Medicine (Baltimore) 2014;93(27):e172.
15. Jezequel P, Kerdraon O, Hondermarck H, *et al.* Identification of three subtypes of triple-negative breast cancer with potential therapeutic implications. Breast Cancer Res 2019;21(1):65.
16. Pundavela J, Roselli S, Faulkner S, *et al.* Nerve fibers infiltrate the tumor microenvironment and are associated with nerve growth factor production and lymph node invasion in breast cancer. Mol Oncol 2015;9(8):1626-35.
17. Asleh K, Negri GL, Spencer Miko SE, *et al.* Proteomic analysis of archival breast cancer clinical specimens identifies biological subtypes with distinct survival outcomes. Nat Commun 2022;13(1):896.
18. Keren L, Bosse M, Marquez D, *et al.* A Structured Tumor-Immune Microenvironment in Triple Negative Breast Cancer Revealed by Multiplexed Ion Beam Imaging. Cell 2018;174(6):1373-1387 e19.
19. Malek M, Taghiyar MJ, Chong L, *et al.* flowDensity: reproducing manual gating of flow cytometry data by automated density-based cell population identification. Bioinformatics 2015;31(4):606-7.
20. Ghandi M, Huang FW, Jane-Valbuena J, *et al.* Next-generation characterization of the Cancer Cell Line Encyclopedia. Nature 2019;569(7757):503-508.
21. Li S, Overman JJ, Katsman D, *et al.* An age-related sprouting transcriptome provides molecular control of axonal sprouting after stroke. Nat Neurosci 2010;13(12):1496-504.
22. Stefansson IM, Raeder M, Wik E, *et al.* Increased angiogenesis is associated with a 32-gene expression signature and 6p21 amplification in aggressive endometrial cancer. Oncotarget 2015;6(12):10634-45.
23. Maman S, Witz IP. A history of exploring cancer in context. Nat Rev Cancer 2018;18(6):359-376.
24. Servick K. War of nerves. Science 2019;365(6458):1071-1073.
25. Lambert AW, Pattabiraman DR, Weinberg RA. Emerging Biological Principles of Metastasis. Cell 2017;168(4):670-691.
26. Mauffrey P, Tchitchek N, Barroca V, *et al.* Progenitors from the central nervous system drive neurogenesis in cancer. Nature 2019;569(7758):672-678.
27. Barretina J, Caponigro G, Stransky N, *et al.* The Cancer Cell Line Encyclopedia enables predictive modelling of anticancer drug sensitivity. Nature 2012;483(7391):603-7.
28. Arnes JB, Stefansson IM, Straume O, *et al.* Vascular proliferation is a prognostic factor in breast cancer. Breast Cancer Res Treat 2012;133(2):501-10.
29. Kruger K, Stefansson IM, Collett K, *et al.* Microvessel proliferation by co-expression of endothelial nestin and Ki-67 is associated with a basal-like phenotype and aggressive features in breast cancer. Breast 2013;22(3):282-8.
30. Nalwoga H, Arnes JB, Stefansson IM, *et al.* Vascular proliferation is increased in basal-like breast cancer. Breast Cancer Res Treat 2011;130(3):1063-71.

Legends

Figure 1. Co-expression and spatial co-localization of neural and vascular markers and structures. **A-B**) Representative IMC images showing co-localization of neural and vascular structures. The images are pseudo colored using the antibody intensity values of Neurofilament (green), CD31/34 (red) and the cytokeratin CKAE1/AE3 (white/grey). Focal co-expression of Neurofilament and CD31/CD34 is observed (yellow); **C-D**) UMAP projection of all endothelial cells found in the cohort of 117 patients. Single-cells are colored based on z-scored Neurofilament expression, and stratified into Ki67-high and Ki67-low groups based on Ki67 antibody intensity; **E**) Boxplot comparing neurofilament intensity in Ki67-high and Ki67-low CD31/CD34-positive endothelial cells ($p < 0.001$); **F**) Boxplot comparing distance of CD31/CD34-positive endothelial cells of Ki67-high and Ki67-low levels from Neurofilament high endothelial cells (log2 transformed; $p < 0.001$). P-values are based on Mann-Whitney U test.

Figure 2. Immunostaining for markers of angiogenesis and neurogenesis and their associations in primary breast cancer (Bergen Breast Cancer cohort, n=461-483). A) Immunostaining with Neurofilament antibody (x400), illustrating the positivity in the microaxons between the cords and glands of tumor tissue; **B**) Presence of thick Neurofilament positive nerve bundles; **C-D**) Dual immunostaining with Factor VIII (red) for endothelial cells and Ki67 (blue) for proliferating cells (x400). Vessels with no proliferative activity in (C), and Ki67 positive proliferating endothelial cells in (D) (highlighted with arrows); **E**) Boxplots showing the Vascular proliferation index (VPI) score across breast cancer cases with or without stromal micoraxons in the primary tumor. **F-G**) High vascular proliferation index (VPI) in the primary tumor, and the presence of proliferating vessels in lymph node metastases associates with reduced cancer specific survival in patients; **H**) Microaxon density (MAD) did not associate with survival in primary tumors; **I**) Presence of microaxons in lymph node metastases associates with reduced breast cancer specific survival. All P values shown in (E) are based on Mann-Whitney U test with '*' <0.05, '**'< 0.01 and '***'< 0.001), NS indicates non-significant results. A log-rank test was used to calculate the p-values in the Kaplan-Meier plots (F-I).

Figure 3. **Differential abundance of neurogenesis-related and angiogenesis-related proteins in breast cancer tissues, cell lines and secretome using mass spectrometry. A**) Volcano plot showing differentially enriched proteins between basal-like and luminal-like tissues. P-values were adjusted using Benjamin-Hochberg method. Down-regulated proteins (green), up-regulated proteins (pink),, angiogenesis-related proteins (dark red), neurogenesis-related proteins (blue), ERBB2 was annotated in both categories (purple); **B)** Heat map presentation of angiogenesis- and neurogenesis-related proteins found in a) using in-house microdissected breast cancer epithelium (n=24); **C)** Publicly-available whole-tissue breast cancer samples (n=289); **D)** CCLE data breast cancer cell lines (n=30); **E)** In-house secretome data (n=12). In all heatmaps the protein expression levels were transformed to an expression scale from 0-1 for comparison purposes.

Figure 4. **Univariate survival analysis of the NAS-43 signature in the Metabric Discovery cohort**. Kaplan-Meier plots showing the probability of survival in patients from the METABRIC-Discovery cohort (n = 939; Normal-like subgroup excluded) **(A,B)** and from the online KMPlotter tool **(C,D)** based on their Neuro-Angio gene signature score. Patients with high score (upper quartile) are shown in red and the rest are shown blue (METABRIC) and black (KMPlotter). A high gene signature score is associated with significantly worse survival in all patients **(A,C)** and in patients with Luminal A breast cancer **(B,D)** (log-rank test $p \leq 0.001$).

Figure 5. Unsupervised signature-clustering separates breast cancer patients into high and low breast cancer specific survival. **A)** Unsupervised Hierarchical clustering of seven breast cancer signatures that are associated with aggressive features revealed four clusters (C1, C2, C3 and C4). The signatures are divided into high and low score. All four breast cancer subtypes are represented in each cluster (C1-C4). **B)** Univariate survival analysis, using the Kaplan-Meier method, shows an association between patient clusters and breast cancer specific survival, with C4 showing the worst survival. **C)** Cox' proportional hazard modelling shows that the C2 and C4 clusters demonstrate independent prognostic value in multivariate survival analysis, adjusting for tumor size, histologic grade, and LN metastasis and the PAM50 intrinsic subtypes, using data from the combined METABRIC cohort.

Tables

Table 1. Associations between presence of axons and clinico-pathologic features of primary tumors (n=483)

Variable	Axons (primary tumor)				
	Absent n (%)	**Present n (%)**	**OR**	**(95% CI)**	**P[C]**
Tumor diameter					0.001
≤ 2 cm	302 (82)	65 (18)	1.0		
>2 cm	79 (68)	37 (32)	2.2	(1.4-3.5)	
Histologic grade					<0.001
Grade 1 - 2	325 (82)	71 (18)	1.0		
Grade 3	56 (64)	31 (36)	2.5	(1.5-4.2)	
Lymph node metastasis					NS
No	281 (81)	68 (19)	1.0		
Yes	96 (74)	33 (26)	1.4	(0.9-2.3)	
ER					0.027
Positive	326 (81)	78 (19)	1.0		
Negative	55 (70)	24 (30)	1.8	(1.1-3.1)	
PR					NS
Positive	270 (81)	65 (19)	1.0		
Negative	111 (75)	37 (25)	1.4	(0.9-2.2)	
HER2 status					0.027
Negative	335 (81)	81 (19)	1.0		
Positive	46 (69)	21 (31)	1.9	(1.1-3.3)	
Ki-67 %[A]					<0.001
Low	291 (85)	53 (15)	1.0		
High	90 (65)	49 (35)	3.0	(1.9-4.7)	
Molecular subtype[B]					
Luminal A	165 (88)	23 (12)			
Luminal B / HER2 -	138 (76)	44 (24)			0.003
Luminal B / HER2+	30 (70)	13 (30)			0.003
HER2 +	16 (67)	8 (33)			0.006
Triple negative	32 (70)	14 (30)			0.002
Basal-like phenotype (CK5/6)					0.09
Negative	336 (80)	84 (20)	1.0		
Positive	45 (71)	18 (29)	1.6	(0.9-2.9)	

n: number of patients; OR: odds ratio; CI: confidence interval; ER: Estrogen receptor; PR: Progesterone receptor; HER2: Human epidermal growth factor 2; CK5/6: Cytokeratin 5/6. [A]Cut-off 30% (upper quartile); [B] St. Gallen 2013; [C]P-values by Pearson's chi-square test. Missing data on lymph node status, n = 5.

Table 2. Associations between markers of vascular proliferation (pMVD, VPI) and clinico-pathologic features of primary tumors (n= 461).

Variable	n (%)	pMVD[D]	P[E]	VPI[D]	P[E]
Tumor diameter			0.007		0.002
≤ 2 cm	344 (75)	2.6		3.07	
>2 cm	117 (25)	4.3		5.97	
Histologic grade			<0.001		<0.001
Grade 1 - 2	378 (82)	2.2		2.78	
Grade 3	83 (18)	7.0		9.62	
Lymph node metastasis[A]			0.033		0.023
No	331 (72)	2.6		3.15	
Yes	127 (28)	4.3		4.13	
ER			<0.001		<0.001
Positive	385 (83)	2.1		2.8	
Negative	76 (17)	7.8		10.8	
PR			<0.001		<0.001
Positive	322 (70)	2.1		2.80	
Negative	139 (30)	5.0		7.47	
HER2 status			0.001		<0.001
Negative	396 (86)	2.6		2.90	
Positive	65 (14)	6.1		8.88	
Ki-67 %[B]			<0.001		<0.001
Low	328 (71)	1.7		2.29	
High	133 (29)	7.4		9.62	
Molecular subtype[C]			<0.001		<0.001
Luminal A	179 (39)	1.3		1.56	
Luminal B/ HER2 -	171 (37)	3.5		4.03	
Luminal B / HER2+	44 (9)	5.0		6.01	
HER2 +	21 (5)	7.0		12.4	
Triple negative	46 (10)	8.5		10.5	
Basal-like phenotype (CK5/6)			<0.001		<0.001
Negative	399 (87)	2.6		3.02	
Positive	62 (13)	6.7		8.83	

n: number of cases; MVD: microvessel density; pMVD: proliferating vascular density; VPI: vascular proliferation index; ER: estrogen receptor; PR: Progesterone receptor; HER2: Human epidermal growth factor 2. [A] Missing information on lymph node metastasis, *n*=3; [B] Cut off: 30% (upper quartile); [C] St.Gallen 2013; [D] Continuous variables (median value reported for each category); [E] Mann- Whitney U test

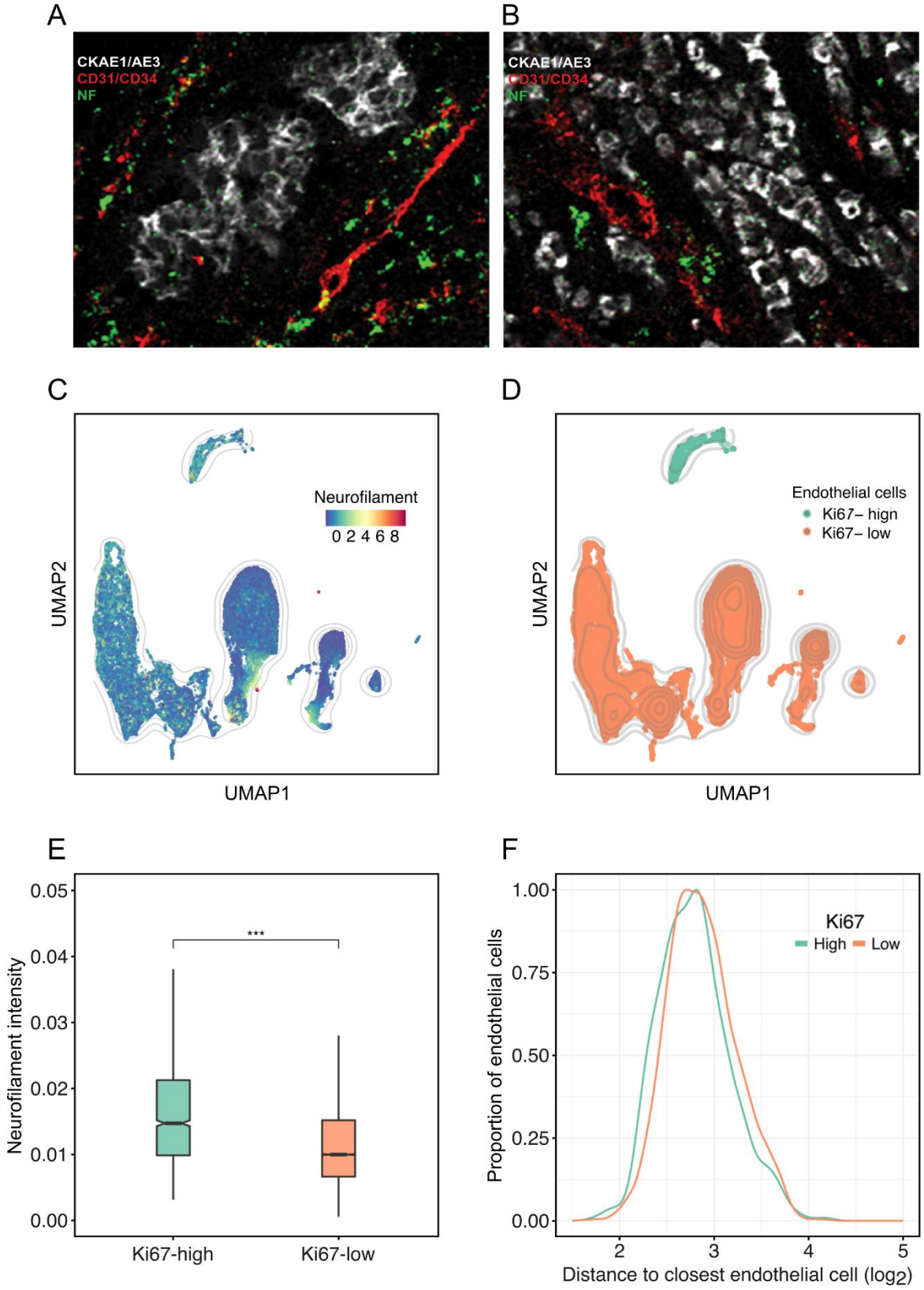
A
CKAE1/AE3
CD31/CD34
NF
B
CKAE1/AE3
CD31/CD34
NF
C
Neurofilament
0 2 4 6 8
UMAP2
UMAP1
D
Endothelial cells
Ki67– hign
Ki67– low
UMAP2
UMAP1
E
Neurofilament intensity
0.05
0.04
0.03
0.02
0.01
0.00
***
Ki67-high
Ki67-low
F
Proportion of endothelial cells
1.00
0.75
0.50
0.25
0.00
Ki67
High
Low
2
3
4
5
Distance to closest endothelial cell (log2)

Figure 1

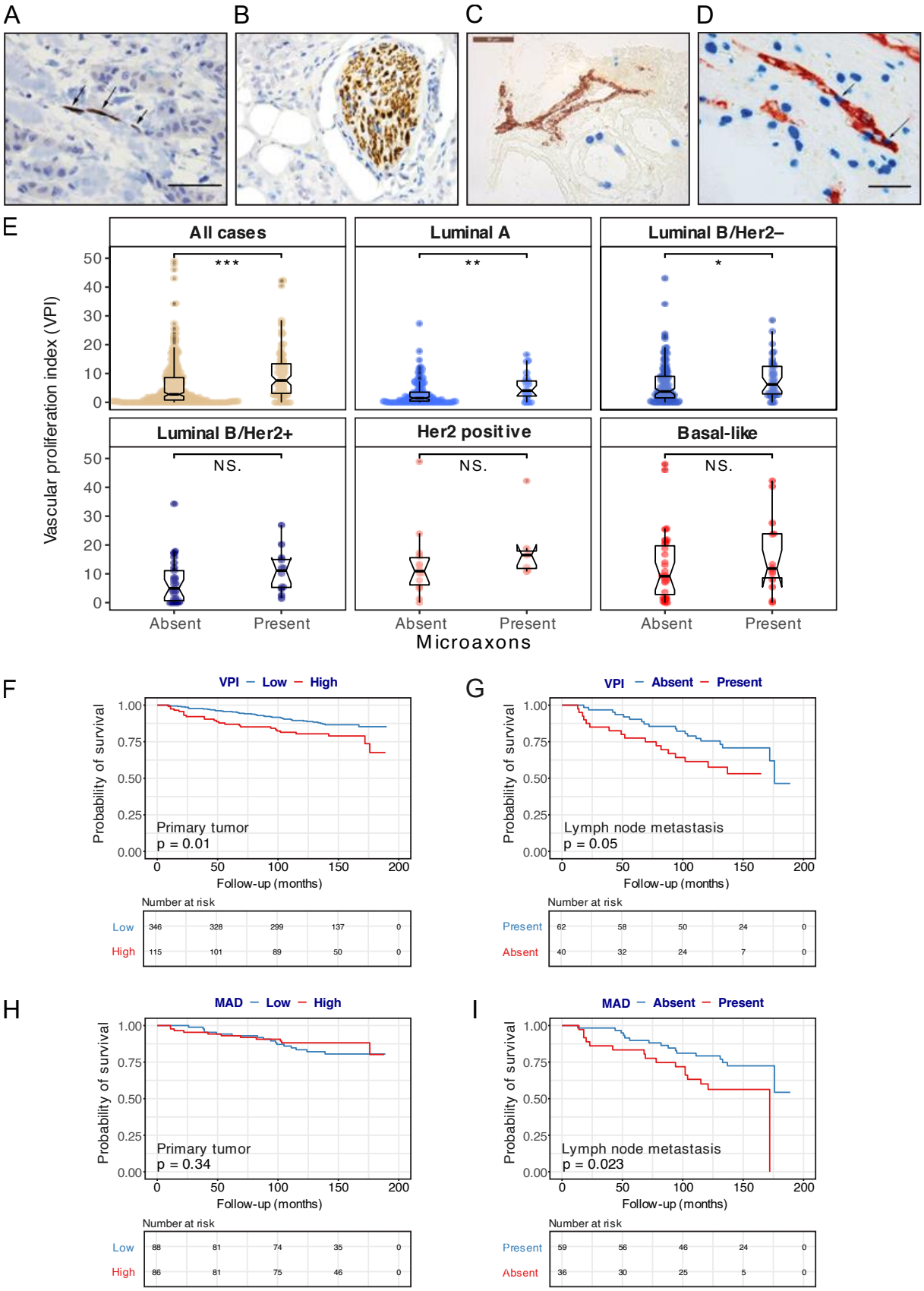
A
B
C
D
E
All cases
Luminal A
Luminal B/Her2–
Luminal B/Her2+
Her2 positive
Basal-like
Vascular proliferation index (VPI)
***
**
*
NS.
Absent
Present
Microaxons
F
VPI – Low – High
Probability of survival
Primary tumor
p = 0.01
Follow-up (months)
Number at risk
Low 346 328 299 137 0
High 115 101 89 50 0
G
VPI – Absent – Present
Lymph node metastasis
p = 0.05
Present 62 58 50 24 0
Absent 40 32 24 7 0
H
MAD – Low – High
Primary tumor
p = 0.34
Low 88 81 74 35 0
High 86 81 75 46 0
I
MAD – Absent – Present
Lymph node metastasis
p = 0.023
Present 59 56 46 24 0
Absent 36 30 25 5 0

Figure 2

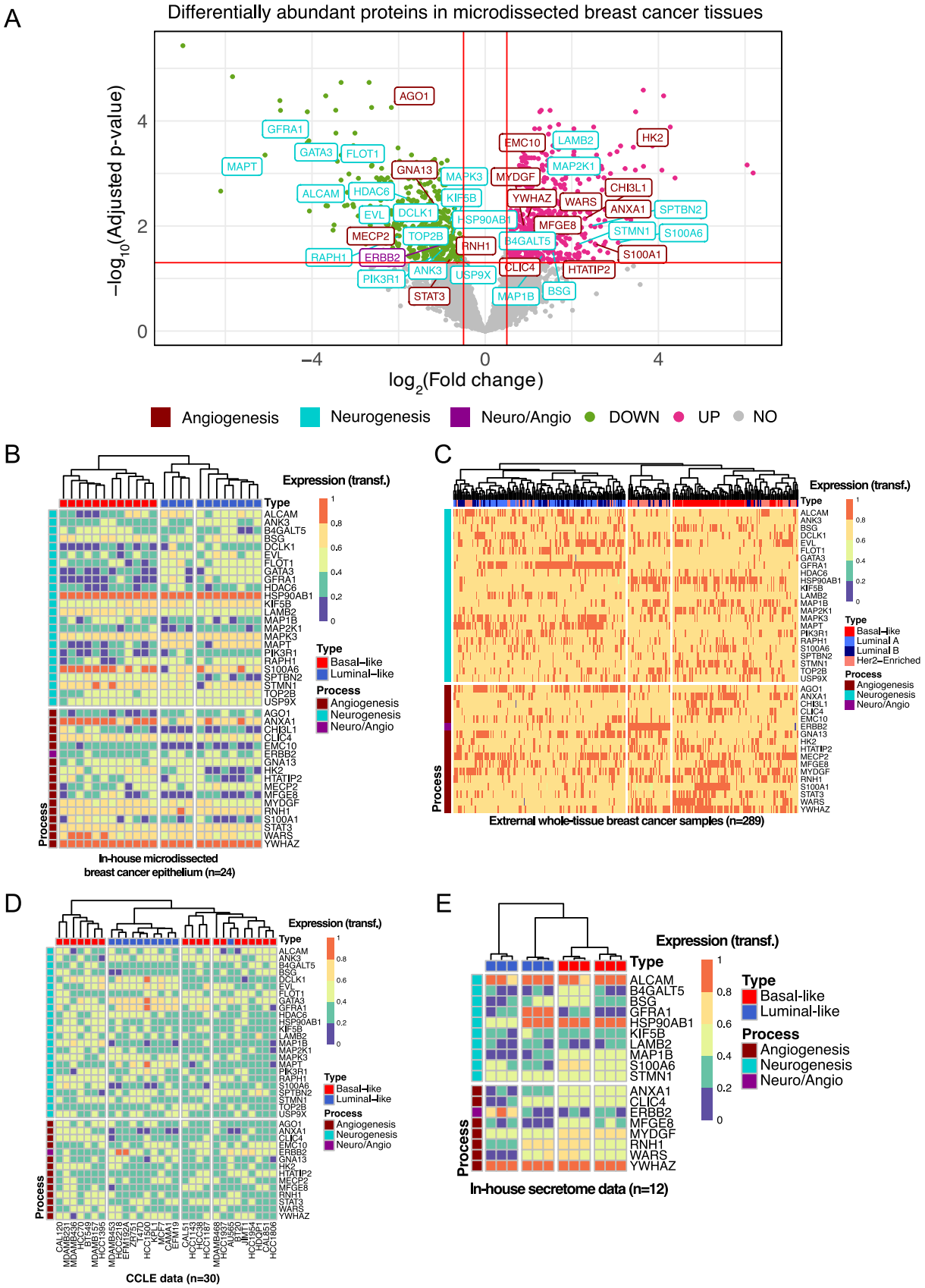
A
Differentially abundant proteins in microdissected breast cancer tissues
−log10(Adjusted p-value)
log2(Fold change)
AGO1
GFRA1
GATA3
FLOT1
MAPT
GNA13
MAPK3
MYDGF
EMC10
LAMB2
HK2
MAP2K1
CHI3L1
ALCAM
HDAC6
KIF5B
YWHAZ
WARS
ANXA1
SPTBN2
EVL
DCLK1
HSP90AB1
MFGE8
STMN1
S100A6
MECP2
TOP2B
RNH1
B4GALT5
S100A1
RAPH1
ERBB2
CLIC4
HTATIP2
ANK3
USP9X
PIK3R1
STAT3
MAP1B
BSG
Angiogenesis
Neurogenesis
Neuro/Angio
DOWN
UP
NO
B
Expression (transf.)
Type
Basal−like
Luminal−like
Process
Angiogenesis
Neurogenesis
Neuro/Angio
In-house microdissected
breast cancer epithelium (n=24)
C
Expression (transf.)
Type
Basal−like
Luminal A
Luminal B
Her2−Enriched
Process
Angiogenesis
Neurogenesis
Neuro/Angio
Extrernal whole-tissue breast cancer samples (n=289)
D
Expression (transf.)
Type
Basal−like
Luminal−like
Process
Angiogenesis
Neurogenesis
Neuro/Angio
CCLE data (n=30)
E
Expression (transf.)
Type
Basal-like
Luminal-like
Process
Angiogenesis
Neurogenesis
Neuro/Angio
In-house secretome data (n=12)

Figure 3

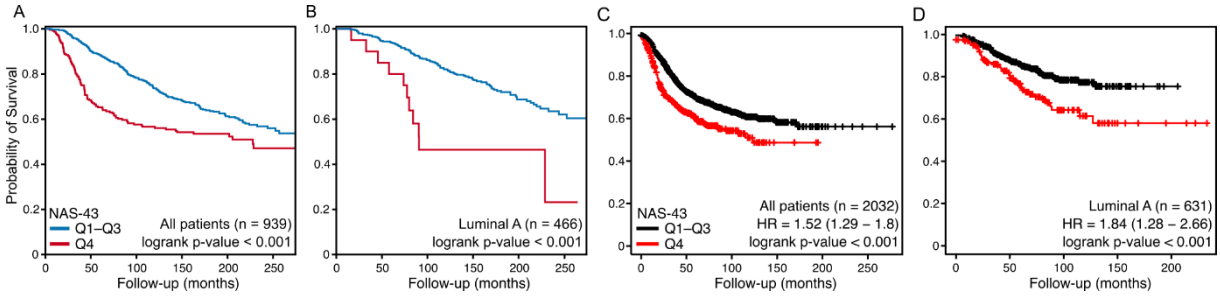
A
B
C
D
Probability of Survival
Follow-up (months)
NAS-43
Q1–Q3
Q4
All patients (n = 939)
logrank p-value < 0.001
Luminal A (n = 466)
logrank p-value < 0.001
All patients (n = 2032)
HR = 1.52 (1.29 – 1.8)
logrank p-value < 0.001
Luminal A (n = 631)
HR = 1.84 (1.28 – 2.66)
logrank p-value < 0.001

Figure 4

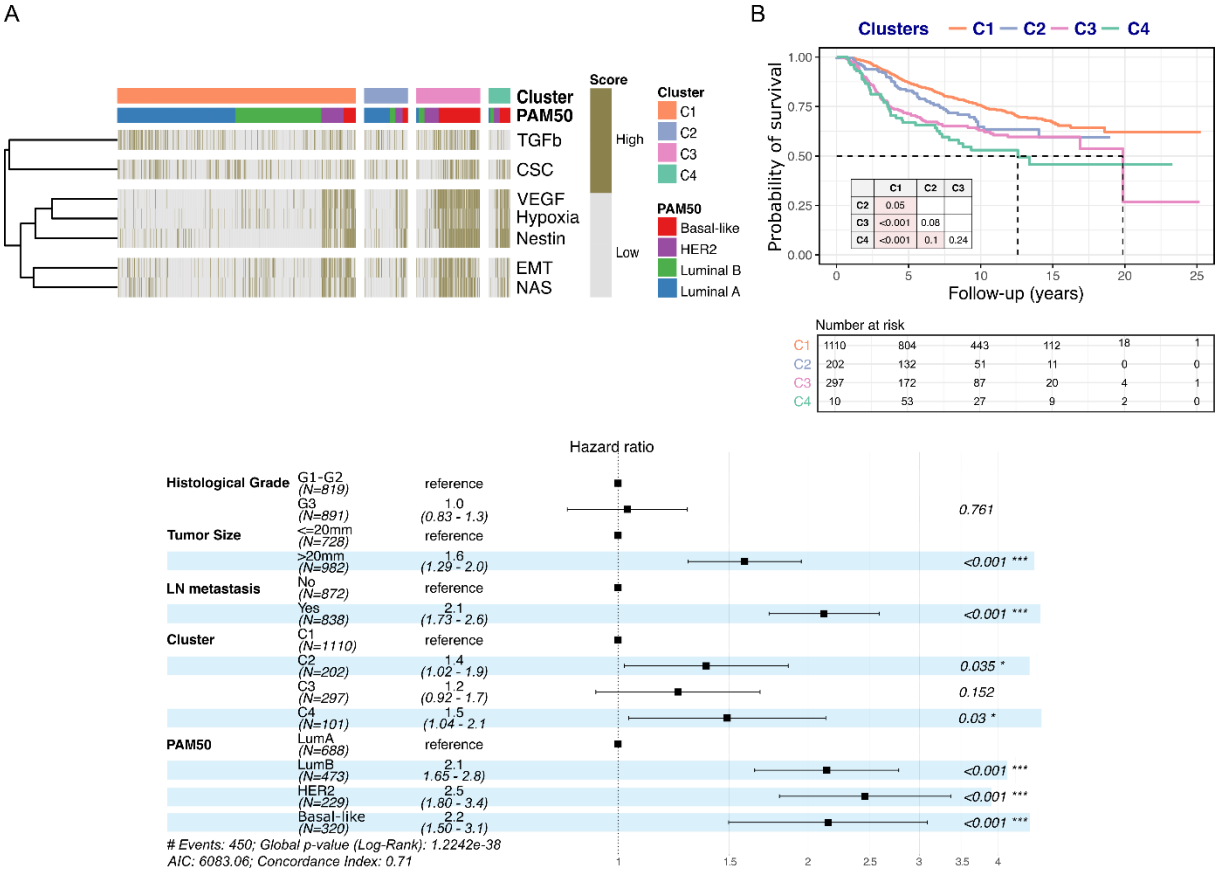
A
Cluster
PAM50
TGFb
CSC
VEGF
Hypoxia
Nestin
EMT
NAS
Score
High
Low
Cluster
C1
C2
C3
C4
PAM50
Basal-like
HER2
Luminal B
Luminal A
B
Clusters C1 C2 C3 C4
Probability of survival
Follow-up (years)
Number at risk
C1 1110 804 443 112 18 1
C2 202 132 51 11 0 0
C3 297 172 87 20 4 1
C4 10 53 27 9 2 0
Hazard ratio
Histological Grade G1-G2 (N=819) reference
G3 (N=891) 1.0 (0.83 - 1.3) 0.761
Tumor Size <=20mm (N=728) reference
>20mm (N=982) 1.6 (1.29 - 2.0) <0.001 ***
LN metastasis No (N=872) reference
Yes (N=838) 2.1 (1.73 - 2.6) <0.001 ***
Cluster C1 (N=1110) reference
C2 (N=202) 1.4 (1.02 - 1.9) 0.035 *
C3 (N=297) 1.2 (0.92 - 1.7) 0.152
C4 (N=101) 1.5 (1.04 - 2.1 0.03 *
PAM50 LumA (N=688) reference
LumB (N=473) 2.1 (1.65 - 2.8) <0.001 ***
HER2 (N=229) 2.5 (1.80 - 3.4) <0.001 ***
Basal-like (N=320) 2.2 (1.50 - 3.1) <0.001 ***
Events: 450; Global p-value (Log-Rank): 1.2242e-38
AIC: 6083.06; Concordance Index: 0.71

Figure 5